IOP Publishing Journal of Optics
J. Opt. 17 (2015) 105002 (8pp) doi:10.1088/2040-8978/17/10/105002

Detection of eccentricity in silver nanotubes by means of induced optical forces and torques

R M Abraham Ekeroth[1,3] and M F Lester[2,4]

[1] Instituto de Física de Buenos Aires Departamento de Física, Facultad de Ciencias Exactas y Naturales, Universidad de Buenos Aires, Ciudad Universitaria, Pabellón I, C1428EHA Buenos Aires, Argentina
[2] Grupo de Óptica de Sólidos-Elfo Centro de Investigaciones en Física e Ingeniería del Centro de la Provincia de Buenos Aires, Instituto de Física Arroyo Seco, Facultad de Ciencias Exactas, Universidad Nacional del Centro de la Provincia de Buenos Aires, Pinto 399 (cp 7000) Buenos Aires, Argentina

E-mail: mabraham@exa.unicen.edu.ar and mlester@exa.unicen.edu.ar

Received 16 April 2015, revised 31 July 2015
Accepted for publication 4 August 2015
Published 24 September 2015

Abstract

In previous works (Abraham *et al* 2011 *Plasmonics* **6** 435; Abraham Ekeroth and Lester 2012 *Plasmonics* **7** 579; Abraham Ekeroth and Lester 2013 *Plasmonics* **8** 1417; Abraham Ekeroth R M and Lester M 2015 *Plasmonics* **10** 989–98), we have conducted an exhaustive study about optical properties of metallic realistic two-dimensional (2D) nanotubes, using an experimental-interpolated dielectric function (Palik 1985 *Handbook of Optical Constants of Solids* (Toronto: Academic Press)). In the case of non-homogeneous metallic shells, we suggested (in a theoretical form) a procedure to detect the non-uniformity of shells in parallel, disperse and randomly oriented long nanotubes (2D system). This detection is based exclusively on the plasmonic properties of the response (Abraham Ekeroth and Lester 2012 *Plasmonics* **7** 579). Here we consider exact calculations of forces and torques, exerted by light on these kinds of nanostructures, illustrating the mechanical effects of plasmonic excitations with one example of silver shell under *p*-polarized incidence. This study continues with the methodology implemented in the previous paper (Abraham Ekeroth R M and Lester M 2015 *Plasmonics* **10** 989–98), for homogeneous nanotubes. The features of the electromagnetic interaction in these structures, from the point of view of mechanical magnitudes, make it possible to conceive new possible interesting applications. Particularly, we point out some results regarding detection of eccentricity in nanotubes in vacuum (when Brownian movement is not taken into account). We interpret the optical response of the realistic shells in the framework of plasmon hybridization model (PHM), which is deduced from a quasi-static approximation. Our integral formalism provides for retardation effects and possible errors is only due to its numerical implementation.

Keywords: plasmonics, forces, torques, nanotubes, electromagnetic interaction, inhomogeneous shells

1. Introduction: inhomogeneous metallic shells

In a previous work [4], we showed numerical studies about the optical forces exerted on homogeneous metallic shells under influence of plasmonic resonant excitations in the structure. The interaction between light and surface plasmons (SPs) can induce forces that are exerted on the system [6, 7]. Optical forces, able to be chosen as near-field observables, reveal more information about the electromagnetic interaction than the obtained by far-field observations.

We have pointed out the importance of using the near-fields to calculate correctly the forces, in order to deduce

[3] Fellow of Consejo Nacional de Investigaciones Científicas y Técnicas CONICET.
[4] Consejo Nacional de Investigaciones Científicas y Técnicas CONICET.

interaction's components and discriminate them from radiation's pressure (scattering force [8, 9]) on these systems. Furthermore, we illustrated with examples of thin homogeneous shells, the size-effects implicit in dielectric metallic function, as those can also influence the results of mechanical variables.

By means of our integral formulation, we can extend the study of forces to include the case of non-homogeneous two-dimensional (2D) shells or nanotubes with symmetry breaking [2, 10–12]. Our formalism provides for an exact tool in order to calculate near-field properties of realistic systems [13]. Apart from some depolarization effects and for possible excitations of resonances in the third coordinate in question [14, 15] (in our problem it is an ignorable coordinate: we have infinite cylinders), this calculation contains the same phenomena as the full three-dimensional (3D) calculation, and hence it permits an understanding of the basic physical processes involved in the near-field optical interaction with low computational cost and without loss of generality.

As in the case of homogeneous nanotubes [1, 3, 16], the plasmonic interaction has been adequately described from the framework of plasmon hybridization model (PHM) [17]. This model approaches us to a physical idea of the process of scattering by complex nanostructures. However, it is only strictly valid for small particles, where a quasi-static approach can be realized. Fortunately, PHM is a good approximation of qualitative features of interaction in 2D [2, 18] and 3D metallic shell structures [10–12], that is, describes correctly far-field spectra and near-field distributions. Some of their results are useful even in greater sizes, where small particle's approximations are no longer valid.

From the point of view of PHM, the plasmonic response of a single metallic shell is conceived as a hybridization of excitations of SPs arising from its two interfaces. For geometric reasons, the shell is considered like a composition of two systems: an infinite cylindrical cavity and an infinitely long solid wire.

The broken symmetry makes it possible the interaction between cavity SPs and the SPs of the solid wire with different multipole orders [12]. These features have been studied for simple shell systems, where a Drude dielectric function is assumed for metals [10–12, 18]. However, the mechanism of interaction in these systems when approaching realistic materials (for instance, taking an interpolation of experimental values for the dielectric function) is not much understood.

In this paper, we explore the mechanical magnitudes (forces and torques) exerted by light on silver inhomogeneous nanotubes, and we show that it is possible to obtain resolution and detailed information about the plasmonic interaction in these structures with symmetry breaking. In particular, we show results from one example of shell that covers general properties of this realistic scatterer at nanoscale. Our results allow us to provide a first approach to the movement of the nanotube under radiation. The nanotube could spin and even be deviated from direction of radiation's pressure (direction of wave propagation), depending on the geometric and constitutive parameters of the problem. Here, we analyze the physical process involved in detail for a nanotube immersed in vacuum.

In order to cover a complete description of the present 2D problem, we need to study the two fundamental polarizations of incident waves. Here we only show results under incidence with *p*-polarization (i.e., magnetic field is parallel to cylinders' axis), where plasmonic excitations can be sustained. In this paper, we show how resonant excitations of plasmons strongly affect the forces and torques that electromagnetic field exerts on the structure. In the paper [4], we showed that interband transitions could also affect these mechanical variables in a measurable form.

Finally, based on our results of torques and forces, we propose some possible applications that could be used for detecting inhomogeneities in shells or nanotubes. In this way, we extend the procedure suggested in the work [2], also indicating the possibility to select nanoparticles with anomalies [19].

We divide this paper in four parts. In the first part, we describe the method used to calculate the optical forces and torques exerted on the particle. We present the methodology and corresponding conventions in the second part, in order to understand the results we present in the third part. Lastly, in the fourth part we conclude the work with the final remarks of the study.

2. Exact integral formulation for calculations of forces and torques

From the Maxwell equations without sources it is possible to arrive, in fully vectorial notation, to the total averaged force $\langle \mathbf{F}(t) \rangle$ transmitted by a time-harmonic electromagnetic field through a closed surface $S = S(V)$ [20]. We consider S as immersed in a medium that cannot support shear stresses [21, 22]. It can be written as

$$\begin{aligned}\langle \mathbf{F}(t) \rangle &= \oint_{S(V)} \left\langle \overleftrightarrow{T}(\mathbf{r}, t) \right\rangle \cdot \hat{\mathbf{n}} \mathrm{d}a \\ &= \oint_{S(V)} \Big\langle \varepsilon_0 \varepsilon_\mathrm{r} (\mathbf{E} \cdot \hat{\mathbf{n}}) \mathbf{E} + \mu_0 \mu_\mathrm{r} (\mathbf{H} \cdot \hat{\mathbf{n}}) \mathbf{H} \\ &\quad - \frac{1}{2} \left(\varepsilon_0 \varepsilon_\mathrm{r} E^2 + \mu_0 \mu_\mathrm{r} H^2 \right) \hat{\mathbf{n}} \Big\rangle \mathrm{d}a; \end{aligned} \tag{1}$$

where $\overleftrightarrow{T}(\mathbf{r}, t)$ is the Maxwell stress tensor [20], $\hat{\mathbf{n}}$ is the normal of S pointing to outward direction, and ε_r, μ_r are the relative constitutive parameters of host medium. This is the resultant time-averaged force over the matter inside the volume V, closed by S. This relation for the optical forces is valid only if we take into account linear phenomena, and if we consider the scattering object as rigid [21].

In a similar way, an expression can be deduced for net mechanical torque $\mathbf{N} = \frac{\mathrm{d}\mathbf{J}_\mathrm{mech}}{\mathrm{d}t}$ over the irradiated structure, where $\mathbf{J} = \mathbf{J}_\mathrm{mech} + \mathbf{J}_\mathrm{field}$ is the total angular momentum and $\mathbf{J}_\mathrm{mech}$ ($\mathbf{J}_\mathrm{field}$) the angular momentum of the matter (field). For a

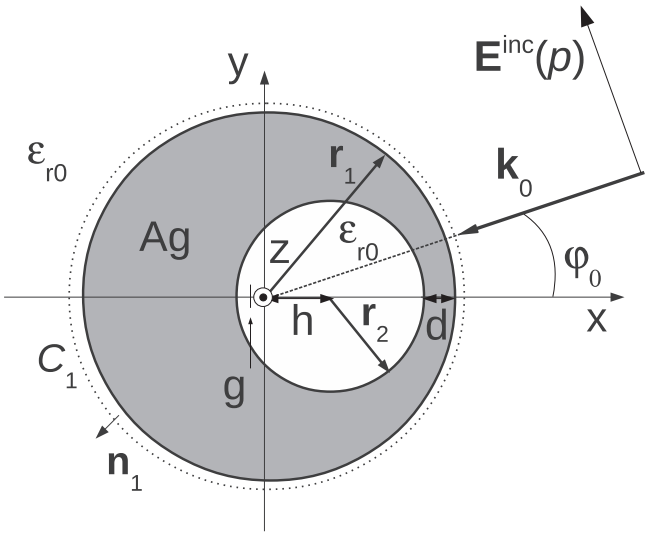

Figure 1. Scheme of used geometry for inhomogeneous 2D-shell problem. We indicate the fundamental polarizations, the coordinate system and the integration contour C_1 for calculations of forces and torques. The homogeneous shell is recovered when $h = 0$. Point g refers to the position of center of mass of the system. The z-axis points perpendicularly outwards the plane of the page. The nanotube is immersed in vacuum ($\varepsilon_{r0} = 1$).

field that satisfies the condition

$$\left\langle \frac{\mathrm{d}}{\mathrm{dt}}\mathbf{J}_{\mathrm{field}} \right\rangle = 0 \tag{2}$$

(see for details [20], for example) the net time-averaged torque, acting over a rigid arbitrary object inside S, is represented by

$$\langle \mathbf{N}(t) \rangle = -\int_{S(V)} \left\langle \overleftrightarrow{\mathbf{T}}(\mathbf{r}, t) \times \mathbf{r} \right\rangle \cdot \hat{\mathbf{n}}(\mathbf{r}) \mathrm{d}a \tag{3}$$

If we consider a 2D problem (axial symmetry with respect to z-axes, and normal incidence lying on the plane (x, y), see figure 1, we can reduce the expression for the time-averaged force, equation (1), in SI units to

$$\begin{aligned}\langle \mathrm{d}_z\mathbf{F} \rangle = \frac{1}{2}\,\mathrm{Re}\Big\{ \oint_{C_j} \Big[&\big(\varepsilon_0\varepsilon_r \mathbf{E}(\mathbf{r}) \cdot \hat{\mathbf{n}}\big)\mathbf{E}^*(\mathbf{r}) \\ &+ \big(\mu_0\mu_r \mathbf{H}(\mathbf{r}) \cdot \hat{\mathbf{n}}\big)\mathbf{H}^*(\mathbf{r}) \\ &- \frac{1}{2}\big(\varepsilon_0\varepsilon_{\mathrm{r}}\,|\mathbf{E}(\mathbf{r})|^2 + \mu_0\mu_{\mathrm{r}}\,|\mathbf{H}(\mathbf{r})|^2\big)\hat{\mathbf{n}}\Big] \mathrm{d}l \Big\}.\end{aligned} \tag{4}$$

The radius $\mathbf{r}$ is contained in the plane (x,y) and we reduce the surface integral to a curvilinear one through $\int_{S_j} \mathrm{d}a = \oint_{C_j} \mathrm{d}l \int \mathrm{d}z$. The contour C_j contains the scatterer j ($j = 1, 2, ..$).

As we assume infinite cylinders, $\int \mathrm{d}z \to \infty$ and we are forced to define a net density of force (NDF)$\mathrm{d}_z\mathbf{F}$ instead of the force $\mathbf{F}$ alone. Similarly, we need to define a net density of torque (NDT) $\mathrm{d}_z\mathbf{N}$ instead of torque, and we deduce from (3) the following equation

$$\begin{aligned}\langle \mathrm{d}_z\mathbf{N} \rangle = \frac{1}{2}\,\mathrm{Re}\Big\{ \oint_{C_j} \Big[&\big(\varepsilon_0\varepsilon_r \mathbf{E}(\mathbf{r}) \cdot \hat{\mathbf{n}}\big)\mathbf{r} \times \mathbf{E}^*(\mathbf{r}) \\ &+ \big(\mu_0\mu_r \mathbf{H}(\mathbf{r}) \cdot \hat{\mathbf{n}}\big)\mathbf{r} \times \mathbf{H}^*(\mathbf{r}) \\ &- \frac{1}{2}\big(\varepsilon_0\varepsilon_{\mathrm{r}}\,|\mathbf{E}(\mathbf{r})|^2 + \mu_0\mu_{\mathrm{r}}\,|\mathbf{H}(\mathbf{r})|^2\big)\mathbf{r} \times \hat{\mathbf{n}}\Big] \mathrm{d}l \Big\}.\end{aligned} \tag{5}$$

Where $\mathbf{N} = N\hat{\mathbf{z}}$. As was opportunely pointed out in paper [4] for forces, equations (4) and (5) are *complete* expressions of respective forces and torques exerted on the structure. For plane waves, the condition (2) is automatically satisfied. For instance, the force of this formulation will contain information about the radiation's pressure exerted on shell and other induced interaction forces. Also note that the NDTs have dimensions of force (N: Newtons in SI units) and the NDFs have dimensions of force/unit length (we choose N nm^{-1}). We obtain the fields involved in equations (4) and (5) by the integral method developed in [1, 2].

3. Methodology and conventions

We show the chosen configuration in figure 1. We use a reference laboratory system of coordinates, denoted as (x, y, z), where z is the ignorable coordinate. The radius of outer (inner) cylinder is r_1 (r_2). The silver shell is simulated by a bulk dielectric function that we have been interpolated from experimental values [5]. The parameter h, which represents the shell eccentricity, displaces the center of inner cylinder to the right, in a form aligned with x-axis. Parameter d is the minimum distance between the interfaces (cylinders). $\mathbf{k}_0$ is the wavevector of the incident wave. The center of the outer cylinder coincides with the origin of (x, y) coordinates. We denote the center of mass of the system with g. An incident plane wave approaches from far field with electric field amplitude $E_0 = 1$ statvolt cm^{-1}, at angle φ_0. As in [4] this value of field corresponds to an intensity of $I_0 = 10^{-3}$ mW μm^{-2}.

In our previous paper [4], we have taken three types of contours for calculations of forces. These three types of results, corresponding to calculations from equation (4) (and now including equation (5)), provide us important information about the electromagnetic interaction in the system. Here we only will use only the contour of integration that closes the shell region from the outside (C_1). We denote the corresponding obtained curves with α, as notation used previously.

It is very important to note that the net force or torque calculated from contour type C_1, also contains information of electromagnetic interaction in the system. The concept that force calculated by contour type C_1 is associated with to radiation's pressure exerted on the particle has to be abandoned in this case. While in the case of homogeneous shell we found that forces calculated by C_1 coincided perfectly with forces calculated by far field approach of radiation's pressure (see equation (2) on the work [4]), in case of

inhomogeneous shell this is no longer true. In section 4 this statement will remain clear.

In the graphics of extinction, forces and torques we use the same symbol and color code (on-line version) for curves, discriminating by angle of incidence. For the sake of simplicity we calculate forces only under incidence with the angles $\varphi_0 = \{0, 45, 90, 135, 180, 225, 270, 315\}^\circ$. The color and symbol codes are always specified in the insets on each figure.

As the response of the structure under *s*-polarization is dominated by interband transitions, similar to case $h = 0$ [4], we do not show it here. We only show results for *p*-polarization. Under this polarization, the electric field lies on the (x, y) plane, see figure 1.

Note that in equation (5) we defined the NDT through the magnitude $\mathbf{r}$, which describes the integration points in question and depends on the chosen reference system. However, we are free to arbitrarily choose the reference point in order to calculate the optical torques at each integration. We will refer to the NDTs calculated with respect to the center of mass of the system (see figure 1). This gives us information about rotation of the 2D particle (spin).

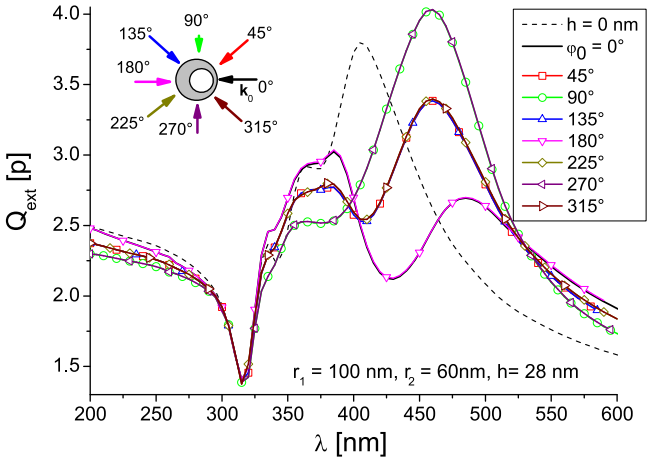

Figure 2. Spectra of extinction efficiencies for inhomogeneous silver shell of $r_1 = 100$ nm, $r_2 = 60$ nm, $h = 28$ nm ($d = 12$ nm) in vacuum under incidence with *p*-polarization. In the inset on the left we show the color code (on-line version) and configuration for different incidence angles (see the right panel for symbol code). As a comparison, we have added the result for special case $h = 0$ ($d = 40$ nm, homogeneous nanotube), curve in dash line. In all the cases, we have used for calculations a bulk metallic dielectric function, interpolated from experimental values of [5].

4. Results

In this section we show results of NDFs and NDTs exerted on inhomogeneous Ag-shells in vacuum, relating them to the optical properties (plasmonic excitations, interband transitions) showed by the typical optical cross sections or efficiencies (far field) [1, 2]. As an example of study, we take a nanostructure with the parameters $r_1 = 100$ nm, $r_2 = 60$ nm, $h = 28$ nm ($d = 12$ nm, shell studied in the work [2]) under the chosen directions of incidence (see previous section). With these parameters, the center of mass is placed at $(-15.75, 0)$ nm with respect to (x, y) defined coordinates [23].

We have pointed out before that this structure has two principal axes associated with the geometry ($\varphi_0 = \{0, 180\}^\circ$ (eccentricity axis) and $\varphi_0 = \{90, 270\}^\circ$) in concordance with our laboratory reference system (see figure 1 for reference).

In order to establish a correlation between far-field results with those from near-fields, which arise from calculations of NDFs and NDTs, we plot the extinction curves for the structure similarly to the analyzed in the work for homogeneous shells [4], figure 2. In order to follow the correlation easily, we have added an inset with the scheme of incidence configuration. We added for comparison, the curve in dash line for extinction due to homogeneous shell, $h = 0$, which naturally does not depend on the incidence angle.

From the figure we can see several plasmonic excitations, which are characteristic for each incidence. In the work [2], we have studied this example of structure and the dynamics of plasmonic resonances in the spectra when varying the incidence angle, mainly for dipolar bonding resonance (low energy peak in the range of $\lambda = (425-550)$ nm). Note the most effective excitation of SPs occurs at incidence angles $\varphi_0 = \{90, 270\}^\circ$; this happens due to a better coupling of electric field (from incident wave) to SPs of the shell [24]. As we observed in the paper [2], this fact makes it possible to know, only from the extinction curves, the position of the main axes of the system (eccentricity between the cylinders lies in one of these axes). However, the extinction curves do not reveal completely the information of the symmetry breaking in the structure. Roughly speaking, we can understand the extinction efficiency as the effective 'shadow' of the illuminated nanotube. Then, the curves of extinction due to a couple of conjugate angles of incidence repeat each other. In this way, we cannot use the extinction to sense direction where eccentricity lies.

Another phenomenon occurs in the spectra at high energy: multipolar excitations of SPs are most effective in the case of incidence with $\varphi_0 = \{0, 180\}^\circ$. These clearly point out a fact we have stated before, that is, multipolar excitations are originated by relative phase-difference of fields at the interfaces of the scatterer. This is connected with its size (retardation effects) and the geometric-induced symmetry breaking on it.

In figures 3 and 4, we show the evolution with the incidence wavelength for x and y components of NDF under several incidence angles. The curves of NDF show a more complex behavior with respect to those from homogeneous shells, even in the situation where incidence conserves specular's symmetry of shell (i.e. $\varphi_0 = \{0, 180\}^\circ$). Analogously, we show in figure 5 the results for NDT. In general, we can appreciate in all the curves the influence of plasmonic excitations on the spectra. The plasmonic response of the system strongly affects the spectra of NDFs and NDTs.

The curves reflect the interactions between the incident wave and SPs and, consequently, an increasing of radiation's pressure in resonant form on the particle. The excitation of SPs can actually deviate the particle in another direction different from forward direction, even we will see that

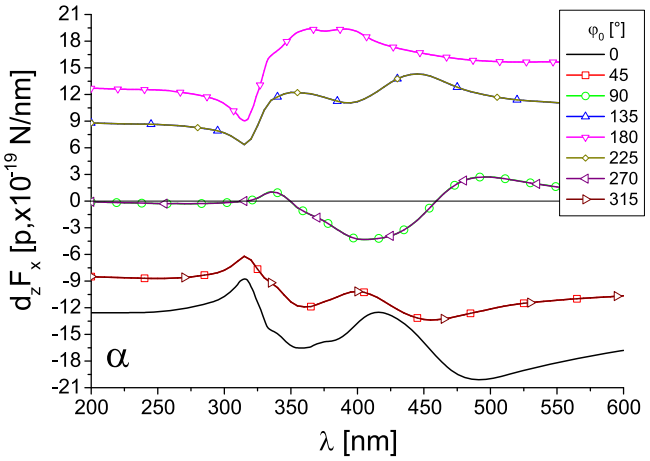

Figure 3. Spectra of x-component of NDFs for the inhomogeneous silver shell of figure 2. We have highlighted the line of zeros of NDF with a thin continuous black line. The notation α means integration on contour type C_1, as used in [4]. We also use it in the following figures.

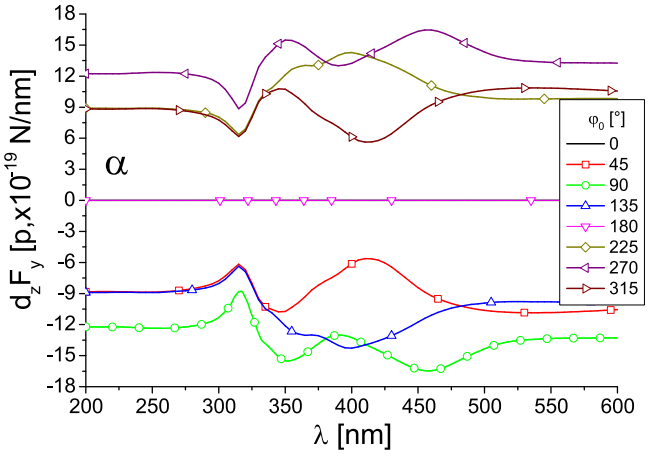

Figure 4. Idem figure 3 for y-component of NDF.

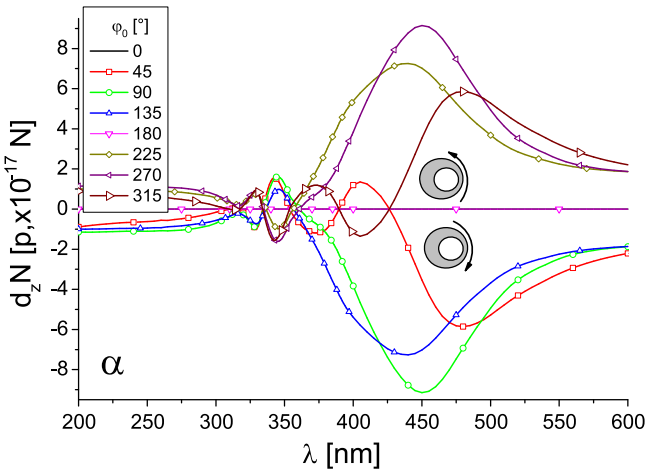

Figure 5. Spectra of NDTs for inhomogeneous silver shell of figure 2. The added schemes indicate the sense of spin of the particle, in agreement with signs of calculated NDTs.

excitation of SPs can make the particle to spin. Furthermore, we also easily recognize the excitations due to interband transitions in the range of short wavelengths ($\lambda \simeq \{200-315\}$ nm). It is the dominant feature for mechanical effects at high energies, giving not vanishing values of NDFs.

We also observe, in general, that the results of forces and torques are able to show the information of the structure 'hidden' on the extinction curves (figure 2). Due to the interaction between light and SPs, they give us information about the details of configuration, such that one in principle can know the direction and sense of eccentricity (or geometrical parameters of the structure). Again, like we found in [4], the resonances of SPs occur at wavelengths slightly different from those found in the extinction spectra. For instance, SP of low energy is excited in Q_{ext} at $\lambda = 485$ nm for $\varphi_0 = 0°$, while in NDF it is found at $\lambda = 493$ nm (red-shift with respect to extinction, like we found in [25]). The spectral position in Q_{ext} for the SP of high energy is $\lambda \simeq 333$ nm; the same spectral position we find in curves of NDF, also for angle $\varphi_0 = 0°$. We associate this SP with the antibonding dipolar one, in agreement with previous studies [12, 18].

Note, as an example, the x-component of NDF for incidence angles $\varphi_0 = \{0, 180\}°$ in figure 3; its corresponding curves in Q_{ext} (figure 2) are equal, but in NDF we can distinguish them. The x-component of NDF for these same incidence angles is distinguishable. Apart from a different sign (the particle would be pushed on opposite directions), when comparing the curves for the absolute values of NDF, they differ notably in the range of excitation of SPs ($\lambda = \{320-600\}$ nm). In the other ranges of wavelength, their absolute values result identical. Their greater difference is placed at excitation of low energy SP ($\lambda \simeq 493$ nm in NDF, figure 3). We associate this SP with the bonding dipolar one [2, 11, 12]. This result is directly related to the detection of eccentricity, using the same incidence angles, by analyzing the scattering efficiency [2]. On the other hand, the curves in figure 3 for the other angles remain degenerate (equal). By symmetry of the system with respect to x-axis, the curves for conjugate angles $\varphi_0 = \{90, 270\}°$ and $\varphi_0 = \{135, 225\}°$ are equal, which results natural. However, if we observe the absolute values of curves for $\varphi_0 = \{45, 135\}°$ or $\varphi_0 = \{135, 315\}°$, the curves again differ notably, but only in the range where SPs dominate the spectra. The curves of absolute values of NDF for the conjugate angles $\varphi_0 = \{45, 315\}°$ naturally result equal.

The most interesting result for this figure is deduced from the curves of $\varphi_0 = \{90, 270\}°$. The x-component for NDF is not null (green line with circles and violet line with triangles) as one could expect intuitively for these angles. Its curves oscillate around zero line of (x-component of) NDF. In fact, this oscillation is produced from excitation of SPs of the structure.

By means of this transversal component of NDF, which depends on the plasmonic interaction in the inhomogeneous nanotube, one can think in a nanotube characterization of shell eccentricities. Note that it can separate, in principle, nanotubes with deformed shells from those with

homogeneous shells: the homogeneous nanotubes would only follow forward direction, due to radiation pressure, while the movement of deformed ones would be affected by an additional transversal component (that depends on the incidence angle and wavelength).

In the region of interband transitions the curves for $\varphi_0 = \{90, 270\}^\circ$ present a vanishing negative contribution to force. In the limit of very short wavelengths as well as in the opposite limit of long wavelengths, the response tends to be zero.

The results of figure 3 are a proof that curves α, obtained by integration of the Maxwell's stress tensor, (4), contain information about the complete interaction in the structure and not only would give us an expression for radiation's pressure [4, 9], as one primarily may think. The radiation's pressure that one could expect is more related to the corresponding curves for $\varphi_0 = \{90, 270\}^\circ$ on figure 4. By correlation with extinction curves, we can obtain the spectral position of mainly dipolar bonding and anti-bonding SPs in the curves for $\varphi_0 = \{90, 270\}^\circ$ on this figure. In those wavelengths ($\lambda = \{495, 335\}$ nm respectively), the x-component for NDF is positive, and negative in the intermediate zone of multipolar plasmonic excitations.

The fact that both curves for $\varphi_0 = \{90, 270\}^\circ$ on this figure are identical, is directly related to the results (for near-fields) showed in figures 7(c) and 7(d) on [2]. The intensity map corresponding to $\varphi_0 = 270^\circ$ is a perfect specular reflection, respect with the horizontal axis, of the map for incidence with $\varphi_0 = \{90\}^\circ$. Unexpectedly, in both cases, the particle would be pushed in the same direction. This result can be understood in the frame of PHM as a close interaction between two particles: the cavity and the solid cylinder (like a dimer) [12, 18].

In addition, we want to note that the curves for $\varphi_0 = \{90, 270\}^\circ$ have spectral positions where the x-component of NDF is equal to zero. These points are approximately, in increasing order of energy, $\lambda = \{459, 349\}$ nm and $\lambda \leqslant 315$ nm. In these points, the particle only would be pushed by radiation's pressure in forward direction, in a similar way as homogeneous shell would do.

In figure 4, we can note the high symmetry of the obtained curves for y components of NDF. The curves for all the conjugate angles, that is, $\varphi_0 = \{45, 315\}^\circ$, $\varphi_0 = \{90, 270\}^\circ$, $\varphi_0 = \{135, 225\}^\circ$, present specular symmetry with respect to the zero line of force. However, as we observed in figure 3, there are couples of values for incidence angles that sense the perturbations originated by symmetry breaking, by means of excitation of SPs. We find, when comparing the curves of absolute values of NDF for $\varphi_0 = \{225, 315\}^\circ$ and their specular curves $\varphi_0 = \{45, 135\}^\circ$, they are distinguishable only in the plasmonic resonance zone. Note their coincidence on the spectral region of interband transitions, and the same can be found in the limit of very long wavelengths (not shown here: at $\lambda = 600$ nm we can still see plasmonic influences on the spectra). From this figure, as in the previous one, we could know where the direction and sense of shell's eccentricity is. Both set of curves, from x- and y-components of the force, detect the precise position of the shell's inhomogeneity.

For the couple of angles $\varphi_0 = \{0, 180\}^\circ$, the y-component of NDF is null (see figure 4), as we can expect by symmetry. There is no unexpected orthogonal component of the force, with respect to incidence direction. We have checked this fact numerically. The calculated values in this case oscillate around $|d_z F_y| \approx 10^{-24} - 10^{-27}$ N nm^{-1}, depending on the specific parameters of the configuration: wavelength, value of dielectric function, etc.

In figure 5, we observe that the results for NDT show more (resolved) information than in the previous curves for NDFs. The curves, although shown very symmetric, resolve more resonances due to excitation of SPs. The curves of absolute values of NDT for conjugate angles ($\{45, 315\}^\circ$, $\{90, 270\}^\circ$, $\{135, 225\}^\circ$, etc) are identical. For all incidence angles studied (except in the cases $\varphi_0 = \{0, 180\}^\circ$) the curves of NDT show oscillations around zero between bonding and anti-bonding excitations. Even studying our realistic problem, where we have strong overlapping resonances, curves of NDT can resolve them in a much better form than curves of NDFs. Actually, the degeneration of curves is completely lifted. The spectral curves of torques are all distinguishable for incidence angles different from the couple $\varphi_0 = \{0, 180\}^\circ$.

As we expected, the NDT is zero for the case of homogeneous shell. It is due to high symmetry of the system. We have checked it numerically; the calculated values of the torque density $d_z N$ oscillate around $|d_z N| \approx 10^{-24} - 10^{-27}$ N (five and eight orders of magnitude under the scale of curves $d_z N$ in case of shells with symmetry breaking, depending on the specific parameters of the problem). For incidence with $\varphi_0 = \{0, 180\}^\circ$, we found the NDT is null with the same numerical error (curve in black continuous line and curve in magenta with down triangles).

In agreement with right-hand rule, positive values of NDT mean the particles to spin counterclockwise, whereas negative values mean the particles to spin clockwise (see inset schemes on the figure).

In the zone of low energy (within the interval $\lambda \simeq (360-600)$ nm for all the curves), the peaks (or dips) of NDTs are the most intense, due to excitations of bonding dipolar SP. Considering the absolute values of NDT, we find the maximum amplitude of the NDT ($d_z N = 9.2 \times 10^{-17}$ N) for incidence with $\varphi_0 = \{90, 270\}^\circ$, at $\lambda = 450$ nm. We find this resonance at $\lambda = 460$ nm in the corresponding curve in Q_{ext}, which means a blue-shift (see figure 2). However, for angles $\varphi_0 = \{45, 315\}^\circ$, we find SP of low energy at $\lambda = 480$ nm (in Q_{ext} is at $\lambda = 460$ nm, red-shift). For the couple $\varphi_0 = \{135, 225\}^\circ$, the spectral position of this SP in NDT is at $\lambda = 440$ nm (blue-shift). This means that the shifts, in spectral positions, of resonances in NDT depend strongly on the incidence angle as extinction curves correspondingly do. The NDT is also very sensible to the incidence angle. The effective excitation of SPs for low energy (dipolar bonding) shifts strongly in wavelengths, That is, spectral positions of maximum or minimum of curves. Note that for the curves of NDFs this fact is not so clear, the NDT is more sensible. This

is like to say the torque is very sensible to the degree of symmetry breaking or eccentricity, similarly to the behavior found in scattering efficiencies in [2].

We can observe, in addition, that the resonances due to bonding dipolar SPs are much stronger in the curves of NDTs than the other resonances we are able to appreciate. The relative difference in amplitude of excitations, when we take into account absolute values of NDT, has been enhanced with respect to the curves of NDFs. We find the spectral position of dipolar antibonding SP in the NDT at $\lambda = 329$ nm for almost all incidence angles. For angles $\varphi_0 = \{135, 225\}^\circ$ we find a slight shift at this resonance; the resonant wavelength is at $\lambda = 330$ (as in extinction) for their two curves.

Note that in the zone of high energies (short wavelengths), as well as in the zone of long wavelengths, the curves of NDT tend to converge to two curves, one for positive values of NDT and the other one for negative values.

The sign of NDT is equal in the dipolar excitations (bonding and antibonding). The oscillating behavior for curves of NDT, in the spectral range between both bonding and antibonding dipolar excitations, is due to excitations of multipolar SPs. If we compare curves of NDT with their corresponding curves in Q_{ext} (figure 2), we could appreciate a correlation between these features of multipolar excitations of SPs.

We can observe, from figure 5, the particular behavior manifested on curves of NDT. The curves for angles $\varphi_0 = \{45, 315\}^\circ$ show more oscillations than in the other curves. We believe they can resolve two more multipolar resonances because under these incidence angles the multipolar response of the shell is enhanced [12, 18]. In particular, as these curves have five relative extrema, and curves of extinction for these angles have four appreciable peaks of resonances (that in general are superpositions of multipolar contributions), we are not able to manage an adequate correlation between them.

In general there are several intervals, depending on incidence angles and wavelengths, where the particle would in principle spin, alternating the sense of rotation. We have said in [4] that these kinds of results are not capable of describing adequately the dynamics of the particle but we can in principle consider them in a *Gedankenexperiment*, as a first approach of the movement of the nanotube. We can imagine, as an example, the dynamics of the system for a fixed wavelength located at the dipolar bonding excitation zone (for instance $\lambda = 450$ nm) for values of angle of incidence different from $\varphi_0 = 0^\circ$ or $\varphi_0 = 180^\circ$. Then the particle undergoes clockwise rotations for angles ($\varphi_0 = 30^\circ, 45^\circ, 90^\circ, .. 135^\circ$), or counterclockwise rotations for angles ($\varphi_0 = 315^\circ, 270^\circ, .. 225^\circ$). At the angles $\varphi_0 = \{90, 270\}^\circ$ the particle experiences the greatest absolute value of NDT (with respect to our coordinate frame; unstable angular positions), while in the angles $\varphi_0 = \{0, 180\}^\circ$ the NDT is zero (stable angular positions).

If we consider initially an incidence angle of $\varphi_0 = 90^\circ$ ($\mathbf{k}_0$ vector along y-axis in figure 1), the particle will rotate clockwise (the torque decreases in intensity) until the axis that contains the eccentricity (initially x-axis) aligns with $\mathbf{k}_0$. At this point, the torque on the particle is zero. However, the particle could continue (by inertia) with its clockwise movement but now the resultant torque is opposite to the movement. Finally, the particle changes their direction of rotation (counterclockwise sense) until again the axis that contains the eccentricity is aligned with the incidence. If there are no drag forces (viscous forces) in the host medium, the particle will oscillate around this axis, like in a torsion pendulum.

There are several wavelengths, these time occurring on all the curves, where the value of NDT is zero. This is analogue to what we found for curves $\varphi_0 = \{90, 270\}^\circ$ for the x-component of NDF. At these spectral positions, the particle is not predicted to spin. If we could experimentally observe the spinning of the particle, from this situation we could not distinguish this shell from a homogeneous one.

The results then could be used to design a filter of particles in a way it distinguishes non-inhomogeneous from homogeneous shells. As obtained NDFs do not always obey the direction of radiation's pressure or incidence, we could think in principle of a kind of *selector* device, which could collect the deformed particles and separate them from homogeneous or highly symmetric ones. Also, we may observe if the particle or shell is spinning or not; this could help to corroborate non-uniformity of shells. In order to do this, we must carefully study the configuration to choose adequately the parameters of incidence.

5. Final remarks

In this paper, we have calculated the NDFs and NDTs exerted by light on one realistic example of inhomogeneous silver infinite nanotube. This study is a complement of works [1, 2, 4] about plasmonic resonances in realistic metallic nanotubes. As an extension from the method developed numerically in [2], in order to detect anomalies in shells of nanotubes, we established an alternative procedure based on analysis of mechanical magnitudes.

In general, we found particular behaviors in both forces and torques optically induced, that are generated by excitations of SPs in the structure. We found that these mechanical observables are very sensitive to the constitutive and geometrical configuration of the system (this last one with respect to incident beam). Our results give us information of the intimate interaction between SPs induced by light. Defined mechanical magnitudes, real observables in principle, provide us more (resolved) information of the structure with respect to far-field observables because we can sense the near-fields (evanescent waves) around the scatterer. As in [4], we can identify the character of bonding or antibonding of SPs (not shown here), even when there is a strong superposition of multipolar features in the realistic problem of shell.

We could give an explanation of anti-intuitive result for the x-component of the force when the nanotube is illuminated along the y-axis (see figure 3). If we think the inhomogeneous nanotube as two interacting particles (a cavity + a solid particle, likewise in plasmon hybridization's model), the non-zero x-component for the force is a result from the

multiple interaction between both particles (as a heterodimer). The internal forces are not balanced, leading to a net force transversal to incidence direction. We may call this resultant force, clearly different from a forward component due to radiation's pressure, 'optical binding force' as it is called in [26] for dimers.

From our results, we can approach the dynamic behavior (in a quasi-static form at least) of the system under influence of plane waves: we can observe that eccentric nanotubes tend to rotate and be pushed simultaneously under an adequate illumination (it depends on the relative angle and wavelength of incidence). Free from any external perturbation (drag forces or Brownian motion), the eccentric nanotube could make an oscillatory movement of rotation about its center of mass, while being pushed in a particular direction (that surges from a composition of scattering force and interaction force). But also, there are particular cases where the torques are zero on the system. In cases of high symmetry, the body is simply pushed into the direction of the incident beam by radiation's pressure.

Finally, from this and the previous work [4], we conclude that it is possible characterize a core–shell system using optical and mechanical observables in a complete form. Furthermore, the information contained in both the forces and torques, makes it possible to give a physical meaning to the multiple interaction between plasmons.

Conflicts of interest

The authors declare that they have no conflict of interest.

Acknowledgments

M L and R M A E thank Teresita Maldonado for reading text and thank to Universidad Nacional del Centro de la Provincia de Buenos Aires and CONICET for funding. R M A E thanks to CONICET for his post-doctoral fellowship.

References

[1] Abraham E R, Lester M, Scaffardi L and Schinca D 2011 *Plasmonics* **6** 435
[2] Abraham Ekeroth R M and Lester M 2012 *Plasmonics* **7** 579
[3] Abraham Ekeroth R M and Lester M 2013 *Plasmonics* **8** 1417
[4] Abraham Ekeroth R M and Lester M 2015 *Plasmonics* **10** 989–90
[5] Palik E D 1985 *Handbook of Optical Constants of Solids* vols I, II, III (Toronto: Academic Press)
[6] Wang N *et al* 2014 *Opt. Lett.* **39** 2399–402
[7] Lehmuskero A *et al* 2015 *ACS Nano* **9** 3453–69
[8] Brzobohatý O *et al* 2015 *Nat. Sci. Rep.* **5** 8106
[9] Van de Hulst H C 1981 *Light Scattering by Small Particles* (New York: Dover)
[10] Wang H *et al* 2006 *Proc. Natl Acad. Sci.* **103** 10856
[11] Knight M W and Halas N J 2008 *New J. Phys.* **10** 1
[12] Wu Y and Nordlander P 2006 *J. Chem. Phys.* **125** 124708
[13] Messina E *et al* 2015 *Opt. Express* **23** 8720–30
[14] Liaw J-W *et al* 2015 *J. Quant. Spectrosc. Radiat. Transfer* **162** 133–42
[15] Xu X, Cheng C, Xin H, Lei H and Li B 2015 *Nature Sci. Rep.* **4** 1–8
[16] Moradi A 2008 *J. Phys. Chem. Solids* **69** 2936
[17] Prodan E and Nordlander P 2004 *J. Chem. Phys.* **120** 5444–54
[18] Moradi A 2009 *Opt. Commun.* **282** 3368
[19] Brzobohatý O *et al* 2015 *Opt. Express* **23** 8179–89
[20] Novotny L and Hecht B 2006 *Principles of Nano-Optics* (Cambridge: Cambridge University Press)
[21] Stratton J 1941 *Electromagnetic Theory* (New York: McGraw-Hill)
[22] Jackson J 1980 *Classical Electrodynamics* 2nd edn (New York: Wiley)
[23] Tipler P A 1995 *Physics for Scientists and Engineers* 3rd edn (New York: Worth Publishers)
[24] Kottmann J P and Martin O J 2001 *Opt. Express* **8** 655
[25] Zuloaga J and Nordlander P 2011 *Nano Lett.* **11** 1280–3
[26] Dholakia K and Zemánek P 2010 *Rev. Mod. Phys.* **82** 1767